Manganese-based room temperature ferromagnetism in gallium arsenide

V. VASILACHE, N. G. APOSTOL[a], G. A. LUNGU[a], D. MACOVEI[a], C. M. TEODORESCU[*,a]
"Stefan cel Mare" University of Suceava, University Str. 13, 720229 Suceava, Romania
[a]National Institute of Materials Physics, P.O. Box MG-7, 077125, Magurele-Ilfov, Romania

Manganese is deposited onto GaAs(001) substrates in high vacuum conditions (10^{-7} hPa), with substrates held at 300 °C. It is shown that this procedure yields to the diffusion of magnanese into gallium arsenide and the formation of a layer which exhibits room temperature ferromagnetism, with highly diluted Mn (below 1 atomic percent). X-ray absorption fine structure determinations at the Mn and Ga K-edges evidenced that Mn is not placed into substitutional Ga sites in GaAs. Most probably, Mn forms MnO clusters with rocksalt local structure. These clusters are the origin of the detected ferromagnetism.

(Received October 22, 2012; accepted October 30, 2012)

Keywords: Manganese, Gallium arsenide, MOKE, Ferromagnetism, X-ray absorption fine structure, EXAFS

1. Introduction

Diluted magnetic semiconductors (DMS) are intensively studied since more than two decades. The original work of Ohno, Munekata and coworkers concentrated on manganese doped GaAs [1-4] and manganese doped InAs [5-7]. In such systems, manganese ions are spaced such as no direct exchange interaction occurs between these ions: the ferromagnetic state is induced by indirect exchange (or RKKY mechanism [8-10]) intermediated by the semiconductor's charge carriers. Therefore, the 'DMS character' stems in the: (i) occurence of ferromagnetic order, with Curie temperature (T_C) as high as possible; (ii) the complete isolation of the magnetic moment carriers [4]; (iii) the mediation of the ferromagnetic order by charge carriers from the semiconductor [8]. If possible, a fourth feature might be added, namely (iv) the possibility of controlling the ferromagnetism via carrier injection, electrically or optically [11,12]. This latter feature could yield to a tremendous range of applications in sensing and remote controlling.

Manganese doped III-V semiconductors (GaAs and InAs), however, failed to show ferromagnetism at a useful temperature for applications (above room temperature). In all the former studies, an upper limit of (T_C) of about 110 K was reported for (Ga,Mn)As [3] and about 30 K for (In,Mn)As [7]. More recently, 150-160 K were reported for (In,Mn)As [13,14] and it seems that Mn-doped gallium nitride have a Curie temperature above room temperature [15]. As a consequence also of the seminal Thomasz Dietl's paper [16], more recent work concentrated on oxides (mainly ZnO and TiO_2) doped with magnetic ions (from Cr to Ni) and the literature of these systems is quite vast [17-19]. However, the simultaneous fulfilment of all requirements (i-iv) from above is rather difficult and the origin of the ferromagnetism in such structures is still a debate [17]. In some cases, oxide superparamagnetic particles are formed [18], whereas in other cases the oxide nanoparticles may exhibit quite useful properties, such as light control of ferromagnetism [19]. However, a major drawback of the doped oxides is related to their relative high bandgap (~ 3 eV), which makes it difficult the generation of charge carriers by optical means, needing energetic photons in the UV spectral range. Also gallium nitride has a bandgap of 3.4 eV. It is therefore desirable to revisit the gallium arsenide case, where the bandgap (1.43 eV) implies that electron-hole generation may be achieved starting with the near-infrared range.

At the same time, all studies performed so far on manganese doped gallium arsenide used rather expensive molecular beam epitaxy techniques, which cannot be a solution for large scale production of such components. It is also desirable to see which are the properties of structures that may be synthesized in low cost conditions, namely in high vacuum instead of ultrahigh vacuum and by using a simpler approach. This work will present such a study, on systems synthesized in less fastidious conditions, where manganese is simply incorporated into gallium arsenide by deposition on substrates held at elevated temperatures (300 °C). These samples will be shown to exhibit a weak ferromagnetism and a complete diffusion of manganese into gallium arsenide; however, a more detailed analysis of the manganese local environment by X-ray absorption spectroscopy will shown that rocksalt MnO clusters are formed; however, these small clusters

have magnetic moments coupled in a ferromagnetic state, with about 2.4 μ_B (Bohr magnetons) of magnetic moment per Mn atom. Therefore, a promising gallium arsenide based material exhibiting ferromagnetism may be synthesized by quite simple means.

2. Experimental details

The preparations were carried out in a home made high vacuum chamber provided with a turbomolecular pump and achieving an ultimate vacuum in the low 10^{-7} hPa range. The substrates are placed on a home made tantalum sample holder with possibilities of heating by electron bombardment. The sample temperatures are determined with an infrared pyrometer. The substrates were ultrasonically cleaned in ethanol at 60 °C. Prior to the deposition, the substrates are heated at 520 ± 30 °C for 15-20 minutes. Previous studies have demonstrated the complete removal of the oxygen from the sample surface by this procedure [14,20]. Manganese is evaporated from a prototype high temperature Knudsen cell with direct resistive heating. The advantage of this device is the high stability and possibility to determine exactly the cell temperature from its electrical resistance as function of the heating current. More details about this new kind of evaporator will be published elsewhere. Nevertheless, the stability of the cell is directly reflected in the evaporation rate of Mn, as calibrated *in situ* with a quartz thickness monitor. Owing to the high versatility of the cell, a constant evaporation rate for Mn was achieved to 1.00 ± 0.02 nm / min related to the bulk Mn parameters.

During the deposition, the substrates were held to 300 ± 20 °C. Previous studies have demonstrated that already at 200 °C manganese completely diffuses into InAs(001) [13,14], whereas Fe forms an alloy with InAs already at 150 °C substrate temperature [21]. Cobalt deposited on GaAs also intermixes and reacts strongly with the substrate, passivated or not [22,23]. In summary, all previous experiences yielded that at temperatures exceeding 250 °C a strong diffusion of the metal into GaAs occurs. These facts pushed us to select the deposition temperature at 300 °C.

After Mn deposition, the samples were capped with a thin layer of 3 nm of Ag for protection against oxidation, then they were taken out from the preparation chamber for other experiments.

Magneto-optical Kerr effect (MOKE) measurements were performed by an AMACC Anderberg and Modéer Accelerator AB setup at room temperature in longitudinal geometry, which means that the applied magnetic field is in the sample plane, and the polarization of the light belongs to the plane defined by the magnetic field and the direction normal to the surface. The setup was previously calibrated such that a Kerr rotation signal of 2.5 mdeg corresponds to 1 nm Fe thickness of bulk iron [24]. This calibration was checked repeatedly on Fe/Si(001) [25,26] and Sm/Si(001) [27], yielding each time consistent results. In the data evaluation, we shall use also the sampling depth of the MOKE method as being of about 20 nm [24,28].

The samples were also tested by X-ray photoelectron spectroscopy XPS (Al K_α, 1486.7 eV photon energy), where almost no Mn 2p signal could be detected. By taking into account that the samples were covered by 3 nm of Ag and considering a photoelectron inelastic mean free path of about 1 nm for electrons of about 840 eV kinetic energy [29], an attenuation factor of exp(-3) ~ 0.05 = 5 % must be employed from signals coming from the substrate (below the Ag later). The method, as it was used for these tests, has a sensitivity of about 0.06 % [30], therefore the Mn concentration near the interface with the Ag layer is below 1.2 at. %.

More accurate determinations of the Mn atomic concentration were performed together with the X-ray absorption fine structure measurements. These experiments were performed at the E4 beamline of the Hasylab synchrotron radiation facility from DESY, Hamburg, Germany. The beamline is installed on a bending magnet. A double crystal Si(111) monochromator was used together with a Au mirror to refocus the beam and cut higher harmonics. In these experiments, fluorescence measurements by using a Si:Li detector was performed.

The ratio between the Mn K_α fluorescence and the Ge K_α fluorescence, normalized with the incoming photon flux, both recorded about the respective photoionization thresholds (6600 eV for Mn and 10400 eV for Ga) was 0.00250, 0.00508, and 0.01063 for samples obtained from an equivalent Mn thickness of 3, 6, and 12 nm deposited on GaAs. To compute the atomic Mn:Ga concentration, one has to renormalize with the fluorescence yield ratio of 0.52:0.33 for Ga:Mn [31] and with the absorption cross section, which scales as $E(\mathrm{K})^{-2.5}$, where E(K) is the energy of the K-edge in question (6535 eV for Mn K-edge and 10360 eV for Ga K-edge). The last proportionality constant may be derived by taking into account that the absorption cross section is proportional to the square of the dipole matrix element:

$$I \alpha | \langle 1s| z |\varepsilon p\rangle |^2 \alpha (Z^{*-5/2})^2 = Z^{*-5} \qquad (1)$$

where Z^* is the effective charge of the initial (1s) state. We take into account also also the dependence of the 1s binding energy as $E(\mathrm{K}) \alpha Z^{*2}$. Therefore, the fluorescence Mn:Ga signals must be multiplied by $0.52{:}0.33 \approx 1.58$ and by $[\mathrm{E(Ga\ K)} / \mathrm{E(Mn\ K)}]^{-2.5} = (6535 / 10360)^{2.5} \approx 0.316$. To get the real atomic concentration [Mn] / [Ga + As], one

has to further divide the [Mn]/[Ga] ratio by two. Finally, the probing depth of the fluorescence signals is not the same for Mn and Ga fluorescence. The penetration depth may be estimated as being proportional to the inverse of the mass absorption coefficient, which is of about 100 cm^2/g at 6 keV and 30 cm^2/g at 100 keV [31]. Finally, it results a correction factor of 0.316 x 1.58 x 3.33 / 2 ≈ 0.831. Therefore, the atomic Mn concentration of the three samples of interest for the present study is 0.208 at. % (3 nm), 0.422 at. % (6 nm), 0.883 at. % (12 nm).

The extended X-ray absorption fine structure spectra are analyzed by using an own program, which was proven in repeated times to be fully compatible with standard EXAFS analysis software [32].

3. Results and discussions

Fig. 1 presents MOKE hysteresis loops obtained at room temperature, in longitudinal geometry. A clear hysteresis loop is presented by the samples with 3 nm an 6 nm, with coercitive fields in the range of 145 Oe.

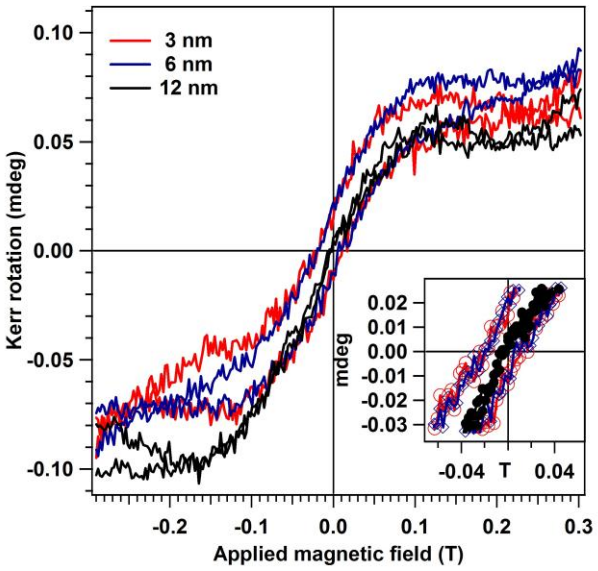

Fig. 1. Magneto-opticall Kerr effect (MOKE) obtained at room temperature on 3, 6 and 12 nm thick Mn deposited on GaAs(001) at 300 °C. The insert represents a low field detail, to highlight the coercitive field.

By a more careful inspection of the insert of Fig. 1, it seems that also a small exchange bias is present, since the coercitive fields in both directions are not equal (+ $H_c \approx 97$ Oe; - $H_c \approx$ - 193 Oe). Nevertheless, if one takes into account also that the hysteresis loop of the 12 nm sample, which does not present any coercitive field, is equally displaced towards negative values by some 49 Oe, we must infer that most probably this displacement is an experimental artifact (connected to remanent fields in the electromagnets, not detected properly by the magnetic field sensor) and not a real effect of to the samples analyzed.

The main result is the presence of a clear hysteresis loop in the most diluted samples and the vanishing of the coercitive field in the sample with the higher Mn content. By taking into account all the MOKE signal calibrations discussed in the previous Section, a Kerr rotation of about 0.1 mdeg, such as the signal exhibited in Fig. 1, would correspond to an atomic magnetic moment of 0.005 μ_B / c, where c is the Mn atomic concentration. From here, a maximum Mn magnetic moment of about 2.4 μ_B is obtained for the most diluded sample. The Mn magnetic moment decreses to about one half of this value for the 6 nm sample (0.4 at. %), and decreases more for the most concentrated Mn sample, together with the disappearance of the coercitivity.

Therefore, the first aim of this work was accomplished, namely the detection of a ferromagnetic signal in Mn-doped gallium arsenide.

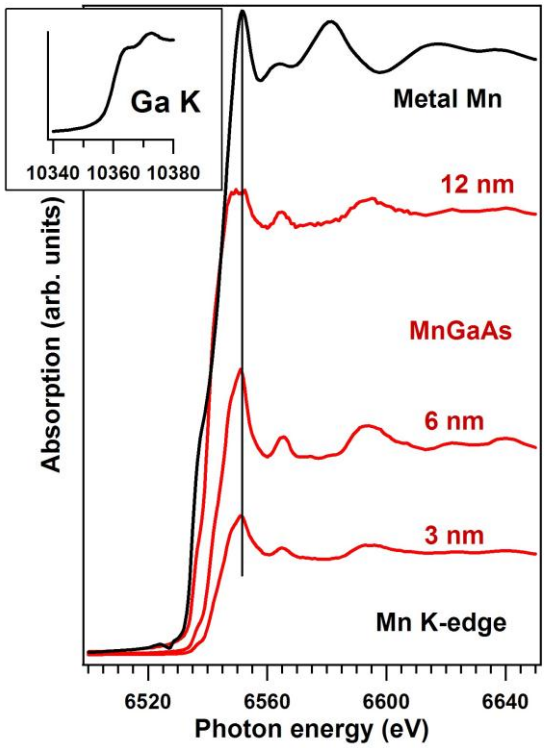

Fig. 2. X-ray near edge absorption spectra at the Mn K-edge of samples consisting in Mn deposited on GaAs at 300 °C, together with the corresponding signal obtained for a Mn thin foil. Note that the MnGaAs samples are covered with a 3 nm layer of silver.

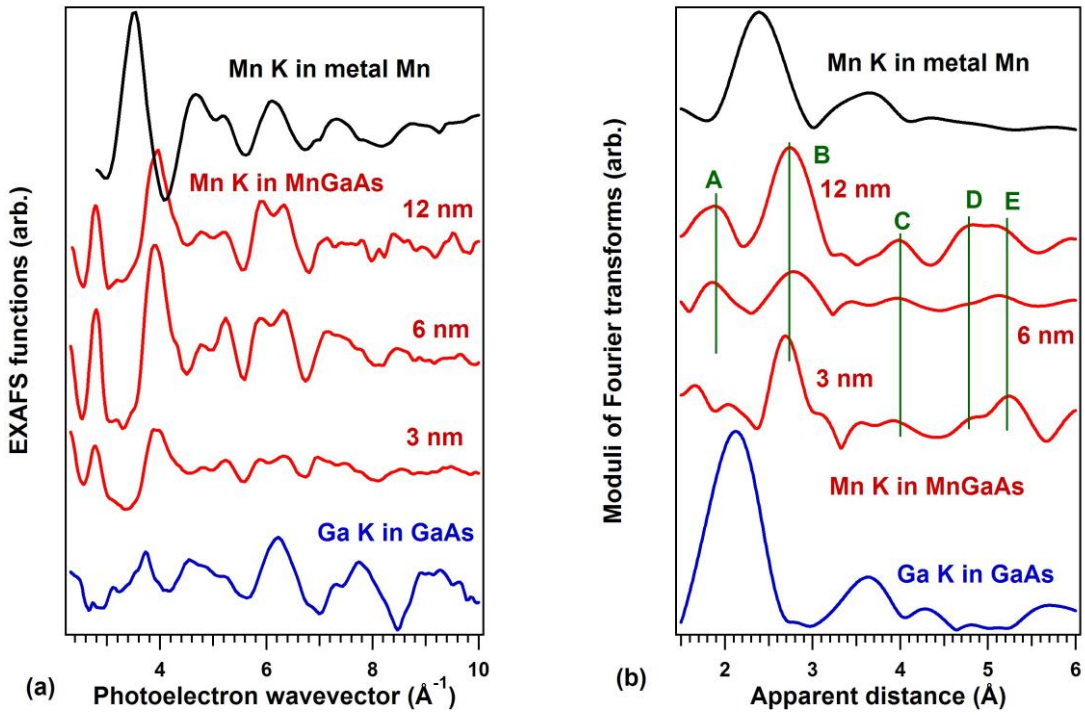

Fig. 3. (a) Extended X-ray absorption fine structure (EXAFS) signalsat the Mn K-edge of MnGaAs samples, of metal Mn and at the Ga K-edge for GaAs; (b) Moduli of the Fourier transforms of the EXAFS functions multiplied by the photoelectron wavevector.

Fig. 2 presents X-ray absorption near-edge (XANES) structure spectra at the Mn K-edge of the MnGaAs samples, together with a spectrum obtained on a Mn thin foil (recorded in transmission, not in fluorescence) and with a Ga K-edge spectrum of a GaAs single crystal wafer. We note from this figure that the MnGaAs XANES is neither similar to the Mn metal spectrum, nor to the Ga K-edge spectrum. Therefore, a simple assertion can be made that neither metal Mn moieties are formed, nor eventual substitution of Ga by Mn. On contrary, the MnGaAs spectra are quite similar to the MnO spectra presented in Ref. [33], especially concerning the distinct fature at 6565 eV. Therefore, a first qualitative conclusion from XANES is that the closest spectrum reported in the literature to be similar to that of the MnGaAs samples is the Mn(II) oxide spectrum.

Fig. 3 presents the extended X-ray absorption fine structure (EXAFS) results. The absorption spectra were recorded on a range up to 600 eV above the absorption edges. Several glitches occured in the spectra, connected to diffraction of incoming X-rays onto different crystalline planes and reflected into the fluorescence detector. These glitches were removed by taking spectra were the fluorescence was detected at different angles (40°, 45° and 50°) with respect to the normal of the sample. The glitches occured at slightly different incoming photon energies for different angles. Therefore, the total absorption spectra were reconstructed by combining regions that did not exhibit glitches. The procedure was quite laborious, but resulted in absorption spectra where only smooth EXAFS oscillations were present.

The next step was to compute the unstructured absorption $\mu_0(h\nu)$ by fitting the whole X-ray absorption by an arctangent threshold [34] together with a Victoreen formula [35]. The EXAFS function $\chi(k) = (\mu - \mu_0) / \mu_0$ was derived, where the photoelectron wavevector is computed as $k = [2m(h\nu - E(\mathrm{K}))\}^{1/2}/\hbar$, where E(K) is the energy of the K absorption edge and the other notations are obvious. For practical reasons, k(Å^{-1}) ≈ 0.51203 x $[(h\nu - E(\mathrm{K})(\mathrm{eV})]^{1/2}$. The EXAFS functions $k\,\chi(k)$ are represented in Fig. 3(a). They are Fourier transformed by using a Hanning window [35]; the moduli of the Fourier transforms are represented in Fig. 3(b).

The EXAFS function may be written as a weighted sum of sine functions:

$$\chi(k) \sim \Sigma_j C_j \sin [2kR_j + \phi_j(k) + \delta_1'(k)] \qquad (2)$$

where the weighting factor C_j contains the number of neighbors in the jth coordination shell, R_j is the radius of this shell, $\phi_j(k)$ the backscattering phase shift, and $\delta_1'(k)$ the phase shift induced by the central atom, which has released the photoelectron after the photoionization process [35]. In absence of these phase shifts, the maxima of the Fourier transform would give directly the interatomic distances corresponding to each shell, R_j. In presence of these phase shifts, only 'apparent' interatomic distances are derived. The complete procedure of the

EXAFS data analysis implies the isolation of a coordination shell, backtransforming in the *k* space, and fitting with appropriate simulations for the scattering and central atom phase shifts, in order to derive correctly the interatomic distances. From Fig. 3(b) it appears that such a procedure would be difficult if one needs to isolate e.g. just the A or the B resonance, especially for the 6 nm layer.

However, in special cases a simplified procedure may be applied. Note also that the manganese oxides were successfully treated by such a simpified procedure [36]. In Fig. 4 we represented the Ga-As and Ga-Ga interatomic distances, as derived from the EXAFS Fourier transform of this work versus the theoretical values obtained from the diamond crystal structure of GaAs with lattice parameter of 5.6535 Å. Also, we represented the Mn-Mn distances: 'apparent distances' from the actual data analysis versus 'true' distances for the Mn bulk crystal structure. Note that the Mn crystal structure is a complicated one and, at least for the first coordination shell, an average distance was used in the graph [37].

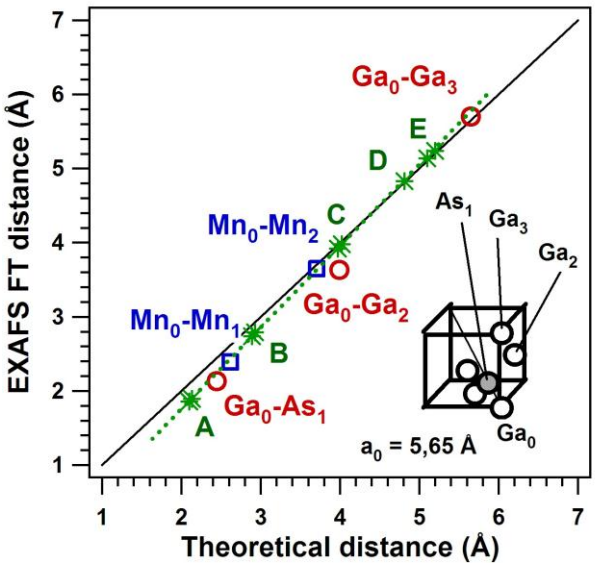

Fig. 4. 'Apparent' distances resulting from the Fourier transforms of the EXAFS functions, as function on the 'real' (crystallographic) interatomic distances: Mn-Mn distances in metal Mn (blue squares); Ga-As and Ga-Ga distances in GaAs (red circles). The black line is the first bisector of the graph. The green dotted line is an attempt to fit the Mn-Mn, Ga-As and Ga-Ga distances. The green stars are the resonances A-E from Fig. 3(b), placed at a convenent 'real' distance, such as to fit on the green dotted line.

All the distances Ga-As, Ga-Ga and Mn-Mn lie on a straight line, represented by a green dotted curve in Fig. 4. On this curve, we inserted the 'apparent' distances of the A, B, C, D and E features from the MnGaAs Fourier transforms from Fig. 3(b), with fitted 'real' distances, such that the points (green stars) lie within ± 0.01 Å on the green dotted calibration line of Fig. 4.

The net results are represented in Table 1. The crystal data for GaAs were used, together with data for Mn(II)O with rocksalt structure, based on the observation from the XANES spectra, especially concerning the resonance at 6565 eV (Fig. 2). In the data interpretation, one has to take into account also the empirical atomic radii of Mn (1.40 Å), O (0.60 Å), Ga (1.30 Å) and As (1.15 Å). The first and most prominent resonance (A) cannot be attributed to any Mn-Ga, Mn-As, or Mn-Mn coordination. This for sure implies coordination with oxygen, both from the derived Mn-O distance in Mn(II) oxide and from the sum of the atomic radii of manganese and oxygen. The second resonance may eventually be attributed to an elongated Mn-Ga coordination or to a contracted Mn-Mn coordination from MnO with rocksalt structure; possibly, also, both configurations coexist. Anyway, Mn-As coordinations may be precluded and this is a good sign for magnetism, since most experimental work demonstrated that 'arsenic is a poison for ferromagnetism' [21,38]. The third resonance (C) may also be attributed to MnO rocksalt structures but, with a good approximation, also to Mn-Ga (second order neighbor) in GaAs with Mn placed on Ga sites. We cannot comment on any definitive attribution for peaks D and E. On one hand, for larger interatomic distances errors due to scattering phase shifts accumulate; on the other hand, multiple scattering may also be important at such distances [37]. And, also, the resonances are not so visible in the Fourier transforms of Fig. 3(b).

Table 1. List of corrected ('real') interatomic distances for the lines observed in the Fourier transform analysis of MnGaAs samples, together with possible interpretations.

Line	'Real' R_j (Å)	Assignment, distances
A	2.11 ± 0.01	Mn-O in MnO: 2.226 Å
B	2.91 ± 0.02	Mn-Mn in MnO: 3.148 Å Mn-Ga in Ga(Mn)As ~ 2.70 Å Mn-As in Ga(Mn)As ~ 2.55 Å
C	4.00 ± 0.03	Mn-O in MnO: 3.856 Å Mn-Ga in Ga(Mn)As: 3.995 Å
D	4.81 ± 0.01	Mn-Mn in MnO: 4.452 Å
E	5.15 ± 0.05	Mn-O in MnO: 4.977 Å

In summary, the XANES data analysis offered the interpretation of Mn(II) oxide, interpretation which was confirmed by the EXAFS data analysis. Eventual discrepancies of the interatomic distances between the corrected experimental values and the theoretical ones obtained from crystallograhic data for resonances A, B and C may also be connected to the fact that oxygen is a much lighter scatterer than Mn, Ga or As; clearly the oxygen scattering phase shift ϕ_O is smaller than ϕ_{Mn}, ϕ_{Ga} or ϕ_{As} and probably further corrections are to be taken into account in computing the 'real' interatomic distances. The placement

of Mn on Ga sites in the GaAs lattice cannot be completely eliminated, namely in what concerns resonance C; in case this happend, it should be accompanied by a first order Mn-As neighboring at about 2.5 Å.

The last question which may be raised concerns the provenience of this oxygen. We recall that the preparations are performed in high vacuum and not in ultrahigh vacuum. In a base pressure of 1×10^{-7} hPa, it is easy to compute that molecules from the residual gas, in a quantity which suffices to form a single atomic layer, will heat the sample surface each ~ 10 seconds. On the other hand, the deposition rate of Mn was around 1.6 Å for each 10 seconds, corresponding roughly to one single atomic layer of Mn. Therefore, oxygen from the residual gas fully reacts with the deposited manganese forming nearly stoichiometric MnO, and this MnO is further diffusing into the GaAs layer. By taking into account the general aspect of the EXAFS oscillations, reflected also in the amplitude of the higher order maxima of the Fourier transform, it seems that these MnO clusters are not that big, possibly they contain only a few elementary cells.

Formation of CoO with rocksalt structure was reported also in the case of another desired DMS, Co-doped ZnO [18]. In that case, however, no room temperature ferromagnetism was observed, and the magnetization curve obtained at low temperatures (2 K) had a very weak ferromanetic component superposed to a superparamagnetic component.

In the actual case, no superparamagnetism was detected even by measuring at higher applied magnetic fields. Therefore, it seems that the MnO entities have a nonzero magnetic momentum, and that these individual momenta are ferromagnetically coupled even at room temperature. Even if this system is not the desired DMS with Mn substituting Ga into teh GaAs crystal structure, one has to remark the presence of the room temperature ferromagnetism, connected to manganese oxide small clusters. Note that MnO is only antiferromagnetic at low temperatures, so the synthesis of ferromagnetic oxidized manganese into GaAs hosts may be regarded as a success of the actual work.

4. Conclusions

Manganese oxide based ferromagnetism was detected at room temperature in gallium arsenide hosts. These samples are prepared in an economical way, namely just evaporation of manganese onto GaAs substrates heated at 300 °C in high vacuum (10^{-7} hPa). Manganese atoms are strongly diffusimg into the GaAs and, together with oxygen atoms from the residual gas, forms MnO nanostructures which are ferromagnetically coupled. It is appealing to propose an RKKY-type mechanism for this ferromagnetic coupling not between individual magnetic moments, but between small clusters carrying a net magnetic moment. For the most diluted Mn-containing sample (about 0.2 atomic %), the Mn atomic magnetic moment was computed to be about 2.4 Bohr magnetons.

XANES and EXAFS methods were proven once more to be the apropriated methods to study such diluted systems. In particular, XANES offered the spectroscopic fingerprints for the presence Mn(II) oxide in the samples, whereas EXAFS may be reasonably interpreted almost exclusively in the framework of a rocksalt MnO structure.

The formation of rocksalt-like oxide clusters when one plans to synthesize diluted magnetic semiconductors was reported earlier, but this is the first time that one detects a measurable ferromagnetic behaviour in such systems. Despite the fact that the MnGaAs system investigated in the present work is not a real 'diluted magnetic semiconductor', it remains, however, a GaAs single crystal -based ferromagnetic system, useful for applications such as in spin injection or other magnetoelectronic devices.

Acknowledgements

The first author (VV) acknowledges the post-doctoral contract No. POSDRU/89/1.5/S/57083. This work is also funded by the IFA-CEA C1-08/2010 and by the PN2-Partnerships 152/2012 Projects.

References

[1] H. Ohno, A. Shen, F. Matsukura, A. Oiwa, A. Endo, S. Katsumoto, Y. Iye, Appl. Phys. Lett. **69**, 363 (1996).
[2] B. Beschoten, P. A. Crowell, I. Malajovich, D. D. Awschalom, F. Matsukura, A. Shen, H. Ohno, Phys. Rev. Lett. **83**, 3073 (1999).
[3] F. Matsukura, H. Ohno, A. Shen, Y. Sugawara, Phys. Rev. B **57**, R2037 (1998).
[4] H. Ohno, Science **281**, 951 (1998); H. Ohno, J. Magn. Magn. Mat. **200**, 110 (1999).
[5] H. Munekata, H. Ohno, S. Von Molnár, A. Segmuller, L. L. Chang, L. Esaki, Phys. Rev. Lett. **63**, 1849 (1989); H. Munekata, H. Ohno, S. Von Molnár, A. Harwit, A. Segmuller, L. L. Chang, J. Vac. Sci. Technol. B **8**, 176 (1990).
[6] H. Ohno, H. Munekata, S. Von Molnár, L. L. Chang J. Appl. Phys. **69**, 6103 (1991); H. Ohno, H. Munekata, T. Penney, S. Von Molnár, L. L. Chang, Phys. Rev. Lett. **68**, 2664 (1992).
[7] H. Munekata, A. Zaslavsky, P. Fumagalli, R. J. Gambino, Appl. Phys. Lett. **63**, 2929 (1993).
[8] M. A. Ruderman, C. Kittel, Phys. Rev. **96**, 99 (1954).
[9] T. Kasuya, Progr. Theor. Phys. **16**, 45 (1956).
[10] K. Yosida, Phys. Rev. **106**, 896 (1957).
[11] S. Koshihara, A. Oiwa, M. Hirasawa, S. Katsumoto, Y. Iye, C. Urano, H. Takagi, H. Munekata, Phys. Rev. Lett. **78**, 4617 (1997); H. Munekata, T. Abe, S. Koshihara, A. Oiwa, M. Hirasawa, S. Katsumoto, Y. Iye, C. Urano, H. Takagi, J. Appl. Phys. **81**, 4862 (1997).
[12] A. Haury, A. Wasiela, A. Arnoult, J. Cibert, S. Tatarenko, T. Dietl, Y. M. d'Aubigné, Phys. Rev. Lett.

79, 511 (1997).
[13] M. C. Richter, P. De Padova, C. Quaresima, P. Perfetti, R. Brochier, V. Ilakovac, O. Heckmann, L. Lechevallier, M. Zerrouki, C. Teodorescu, C. S. Fadley, N. Hamdan, K. Hricovini, J. Alloys Compds. **362**, 41 (2004).
[14] C. M. Teodorescu, M. C. Richter, K. Hricovini, J. Optoelectron. Adv. Mater. **8**, 1200 (2006).
[15] F. Zhang, N. F. Chen, X. Liu, Z. Liu, S. Yang, C. Chai, J. Cryst. Growth **262**, 287 (2004).
[16] T. Dietl, H. Ohno, F. Matsukura, J. Cibert, D. Ferrand, Science **287**, 1019 (2000).
[17] J. M. D. Coey, M. Venkasetan, C. B. Fitzgerald, Nat. Mater. **4**, 173 (2005).
[18] J. Neamtu, G. Georgescu, T. Malaeru, N. G. Gheorghe, R. M. Costescu, I. Jitaru, J. Ferré, D. Macovei, C. M. Teodorescu, Digest J. Nanomater. Biostr. **5**, 873 (2010).
[19] R. M. Costescu, G. A. Lungu, G. Socol, N. G. Gheorghe, D. Macovei, C. C. Negrila, C. Logofatu, M. A. Husanu, D. G. Popescu, C. A. Tache, C. M. Teodorescu, Dig. J. Nanomater. Biostr. **7**, 73 (2012).
[20] C. M. Teodorescu, D. Luca, Surf. Sci. **600**, 4200 (2006).
[21] C. M. Teodorescu, F. Chevrier, R. Brochier, V. Ilakovac, O. Heckmann, L. Lechevalier, K. Hricovini, Eur. Phys. J. B **28**, 305 (2002).
[22] C. M. Teodorescu, J. Chrost, H. Ascolani, J. Avila, F. Soria, M. C. Asensio, Surf. Rev. Lett. **5**, 279 (1998).
[23] M. Izquierdo, M. E. Dávila, J. Avila, H. Ascolani, C. M. Teodorescu, M. G. Martin, N. Franco, J. Chrost, A. Arranz, M. C. Asensio, Phys. Rev. Lett. **94**, 187601 (2005).
[24] V. Kuncser, W. Keune, U. von Hörsten, G. Schinteie, J. Optoelectron. Adv. Mater. **12**, 1385 (2010).
[25] N. G. Gheorghe, M. A. Husanu, G. A. Lungu, R. M. Costescu, D. Macovei, C. M. Teodorescu, J. Mater. Sci. **47**, 1614 (2012).
[26] N. G. Gheorghe, M. A. Husanu, G. A. Lungu, R. M. Costescu, D. Macovei, D. G. Popescu, C. M. Teodorescu, Digest J. Nanomater. Biostruct. **7**(1), 373 (2012).
[27] N. G. Gheorghe, M. A. Husanu, G. A. Lungu, D. Macovei, I. Pintilie, C. M. Teodorescu, J. Mater. Sci. **47**, 7225 (2012).
[28] http://www.uksaf.org/tech/moke.html
[29] S. Hüfner, Springer, Berlin (2003).
[30] The sensitivity S is related to the total number of counts recorded N such as $2S \approx N^{-1/2}$. Survey XPS spectra yielded a maximum intensity of 120,000 cps on a freshly evaporated Mn film. Such survey spectra recorded during 10 seconds yielded a noise level equal to an hypothetical signal provided by a sample with a virtual atomic concentration of 0.6×10^{-3} atomic Mn.
[31] X-ray data booklet, Center for X-ray Optics and Advanced Light Source, Lawrence Berkeley National Laboratory, http://xdb.lbl.gov/xdb.pdf, 2011 release.
[32] A. Negoi, S. Wuttke, E. Kemnitz, D. Macovei, C. M. Teodorescu, V. I. Parvulescu, S. M. Coman, Angew. Chem. Intl. Ed. **49**, 8134 (2010).
[33] B. Gilbert, B. H. Frazer, A. Belz, P. G. Conrad, K. H. Nealson, D. Haskel, J. C. Lang, G. Srajer, G. De Stasio, J. Phys. Chem. A **107**, 2838 (2003).
[34] C. M. Teodorescu, R. C. Karnatak, J. M. Esteva, A. El Afif, J. P. Connerade, J. Phys. B: At. Mol. Opt. Phys. **26**, 4019 (1993).
[35] B. K. Teo, EXAFS: Basic Principles and Data Analysis, Springer, Berlin, 1983.
[36] C. Mande, A. P. Deshpande, Phys. Stat. Solidi B **158**, 737 (1990).
[37] D. Macovei, C. M. Teodorescu, Rev. Roum. Phys. **36**, 945 (1991).
[38] D. J. Singh, J. Appl. Phys. **71**, 3431 (1992).

*Corresponding author: teodorescu@infim.ro